Diagnosing Present and Future Permafrost from Climate Models

Andrew G. Slater[1] and David M. Lawrence[2]

1 National Snow and Ice Data Center, Cooperative Institute for Research in Environmental Sciences, University of Colorado, Boulder, Colorado, USA

2 National Center for Atmospheric Research, Boulder, Colorado, USA

Submitted to
Journal of Climate
June, 2012

Revised, January, 2013
Accepted February, 2013

Corresponding Author:

Andrew G. Slater
National Snow and Ice Data Center, CIRES
University of Colorado at Boulder
Boulder, CO 80309-0449

Tel: 303-735-5358
Fax: 303-492-2468
Email: aslater@kryos.colorado.edu

Abstract

Permafrost is a characteristic aspect of the terrestrial Arctic and the fate of near-surface permafrost over the next century is likely to exert strong controls on Arctic hydrology and biogeochemistry. Using output from CMIP5 climate models, we assess their ability to simulate present-day and future permafrost. Permafrost extent diagnosed directly from each climate model's soil temperature is a function of the modeled surface climate as well as the ability of the land surface model to represent permafrost physics. For each CMIP5 model we separate these two effects by using indirect estimators of permafrost driven by climatic indices and compare them to permafrost extent directly diagnosed via soil temperatures. Several robust conclusions can be drawn from our analysis. Significant air temperature and snow depth biases exist in some model's climates, which degrade both directly and indirectly diagnosed permafrost conditions. The range of directly calculated present-day (1986-2005) permafrost area is extremely large (~4 to 25×10^6 km^2). Several land models contain structural weaknesses that limit their skill in simulating cold regions subsurface processes. The sensitivity of future permafrost extent to temperature change over the present-day observed permafrost region averages $1.67(\pm0.7)\times10^6$ $km^2/°C$ but is a function of the spatial and temporal distribution of climate change. Due to sizable differences in future climates for the RCP emission scenarios, a wide variety of future permafrost states is predicted by 2100. Conservatively, the models suggest that for RCP4.5, permafrost will retreat completely from the present-day discontinuous zone. Under RCP8.5, permafrost will be most probable only in the Canadian Archipelago, Russian Arctic coast and East Siberian uplands.

1 Introduction

Permafrost forms an integral part of the terrestrial Arctic system as well as in the "third pole" of the Tibetan Plateau. A permanently frozen soil matrix and an active layer that experiences annual freeze-thaw cycles can have a particularly large impact on hydrologic fluxes [*Rouse et al.*, 1997; *Yoshikawa and Hinzman*, 2003; *Smith et al.*, 2005] as well as upon flora [*Lloyd et al.*, 2003; *Christensen et al.*, 2004], fauna [*Clark et al.*, 1997; *Wrona et al.*, 2006], geomorphology [*Rowland et al.*, 2010] and biogeochemical cycling [*Schuur et al.*, 2008, 2009]. Socio-economic impacts of permafrost degradation may also prove costly [*Larsen et al.*, 2008]. Permafrost degradation has recently been observed in many locations including Sweden [*Akerman and Johansson*, 2008], Canada [*Fortier et al.*, 2007; *Thibault and Payette*, 2009], Alaska [*Jorgenson et al.*, 2006] and Tibet [*Cheng and Wu*, 2007]. Ground temperatures are warming across the majority of permafrost regions [*Romanovsky et al.*, 2010] and occasionally large rapid changes are seen [*Oberman*, 2008]. Though observations of ground temperature are limited in space, there is a strong indication that permafrost is warming and thawing across much of the permafrost domain in response to recent climate change which raises the question - how much and how fast will permafrost thaw over the course of the 21st century if the climate continues to warm?

Currently, the best tools for peering into Earth's potential future climate are coupled global climate models (CGCMs) or "Earth system models". These models typically constitute fully coupled atmosphere, ocean, land, sea ice and often biogeochemical components. The fifth phase of the Coupled Model Intercomparison Project (CMIP5;

http://cmip-pcmdi.llnl.gov/cmip5/) has brought together CGCMs from international groups to perform a series of coordinated experiments that project future climate based on scenarios of anthropogenic influences. Based on results from climate models several prior efforts have performed assessments of future permafrost in limited regions [*Sazonova and Romanovsky*, 2003; *Zhang et al.*, 2008] or for single climate models [*Stendel and Christensen*, 2002; *Lawrence and Slater*, 2005; *Saito et al.*, 2007; *Lawrence et al.*, 2008] or for periods up to 2050 [*Anisimov et al.*, 1997, *Dankers et al.*, 2010]. While there is agreement across these studies that permafrost degradation will occur with a warming climate, the extent and rate of the process is highly debated.

Our aim in this study is to assess the present state and future trajectory of permafrost within the CMIP5 CGCMs. We also strive to isolate the influence of the simulated model climate from that of each CGCM's embedded land surface model in terms of the diagnosed present-day conditions and future fate of permafrost. In the following sections we introduce the data and methods of diagnosing permafrost, both directly from soil temperatures and indirectly using simplified models. We then assess the CMIP5 model climates over present-day permafrost regions, compare different diagnoses of permafrost, suggest reasons for particular model results and lastly show where permafrost degradation is likely to occur under climate warming scenarios.

2 Data

Monthly mean data is used from reanalysis projects and the collection of CMIP5 climate models. Only the Northern Hemisphere is considered. All data is from grid boxes with greater than 30% land fraction. Glacier points are removed from the analysis and land fractions are accounted for in coastal regions. We use as many models as possible for each portion of our analysis, thus the number used can differ due to data availability.

2.1 Reanalysis Data

As a test of the permafrost diagnostics in the present-day climate, four recent reanalysis products, ERA-Interim [*Dee et al.*, 2011]; NASA-MERRA [*Rienecker et al.*, 2011]; NOAA CFSRR [*Saha et al.*, 2010] and JRA [*Onogi et al.*, 2007] were used. These reanalyses start at the beginning of the satellite period, 1979, and are updated to 2011 and beyond.

2.2 Climate Model Data

Historic and future simulations by coupled climate models were obtained from the CMIP5 archive. A summary of the models included in this study is given in Table 1. We use the CMIP5 simulation designated as *Historical*, and the Representative Concentration Pathway (RCP) cases *RCP2.6*, *RCP4.5*, *RCP6.0* and *RCP8.5*. The Historical simulations run from 1850 or 1860 through to the end of 2005 and are forced with observed changes in atmospheric constituents (CO_2, O_3 etc.) due to anthropogenic or volcanic forcing. The RCP simulations apply an expected increase in radiative forcing e.g. RCP8.5 assumes an extra 8.5Wm^{-2} forcing by 2100. RCP cases go from 2006 until 2099 and were stitched to the end of their respective Historical run. Not all models provided required variables for

all simulations, particularly for non-core CMIP5 cases (e.g. RCP2.6 and RCP6). Full details of the CMIP5 simulations are available from *Taylor et al.* [2009]. Model variables used here are surface air temperature (equivalent to 2m temperature), snow mass, snow depth and soil temperatures (CMIP5 variables TAS, SNW, SND and TSL respectively).

When diagnosing permafrost directly from modeled soil temperatures and making comparisons to simplified models (Section 3.2), we use only the first ensemble member reported by each group (i.e. simulation "*r1i1p1*") and each model maintains its native grid. For present-day assessment of model climates (Section 4.1) and projections based on climatic change (see Section 5) we a) averaged climate variables across all ensemble members (up to 10) for each model and b) interpolated data onto a common grid (that of CCSM4, 0.9°×1.25° degrees, the highest resolution model available) to allow for homogenous comparison.

2.3 Observations: The IPA Map

The International Permafrost Association (IPA) map [*Heginbottom et al.*, 1993; *Brown et al.*, 1997] is perhaps the best available data of permafrost distribution at the global scale. Data used in its compilation dates from 1960 to 1993; in some marginal permafrost regions degradation may have since occurred.

For purposes of comparison, the IPA data was transformed from its 25-km EASE grid onto the common CCSM4 grid by area weighting the occurrence of continuous, discontinuous, isolated or sporadic permafrost. Models currently cannot represent sub-

grid scale permafrost distributions hence in this study we only use the discontinuous and continuous zones in all analysis (i.e., where we expect 50% or more of the ground to be underlain by permafrost) and exclude glaciers. We refer to this 16.2×10^6 km^2 region (blue areas in Figure 1) as the "present-day permafrost area". This model equivalent permafrost area differs from those reported by [*Zhang et al.*, 2000], but is more appropriate for model evaluation.

3 Permafrost Diagnostic Methods

Permafrost can be diagnosed directly from the CMIP5 modeled soil temperatures or indirectly using simplified permafrost models. Modeled soil temperatures are a function of both the simulated surface climate and the ability of the land model to represent permafrost. To separate these two factors and give insights into causes of particular CMIP5 model results we make use of simplified permafrost models that are driven primarily by climate variables.

3.1 Direct Diagnosis of Permafrost from Modeled Soil Temperature (TSL)

For those models that provide soil temperatures, "near-surface" permafrost can be diagnosed as such: if soil at a depth within 3.5m of the surface (based on the lower boundary of a model's soil layers) maintains a temperature of 0°C or less for the present and prior year, it is considered to contain permafrost. This definition (designated here as "TSL") was chosen because active layers rarely reach this depth and it is within the range

of most model soil depths. There is a large range of complexity in land surface models within CMIP5, for example, soil/ground column depths span 3m to 47m, with 3 to 23 soil layers (Figure 2). Horizontal resolutions are similarly variable, ranging from 2.8° × 2.8° to 0.9° × 1.25° (Table 1).

An alternative diagnosis of permafrost sustainability is the annual mean soil temperature (MST) at some depth, say 3.5m, below the surface. If MST is below 0°C and assuming constant soil heat capacity, it is suggestive of permafrost at some deeper depth. Such a diagnostic can ameliorate issues created by coarse soil column discretization within land models. TSL and MST diagnose extremely similar permafrost areas except in the case of three models which show a substantial difference: CanESM2, GISS-E2-R and MPI-ESM-LR (discussed further in Section 4.2.1). Averaged across the present-day permafrost region, modeled values of MST differ greatly (see Table 1). However, MST is not an explicit definition of permafrost nor it does inform about the upper soil state which is important for hydrology, biology and biogeochemical cycling..

3.2 Indirect Diagnosis via Simplified Permafrost Models

We apply two diagnostic models - the Surface Frost Index (SFI) and the Kudryavtsev Method (KUD) - both described below. These models require climatic inputs of annual maximum temperature, annual minimum temperature and mean winter snow depth to generate an annual sinusoidal steady-state climate. The models give equilibrium-type solutions; hence these three climate inputs are averaged for the 20 years prior to the year

for which diagnostics are presented (e.g., the year 2000 uses data averaged over 1981-2000). As these models provide equilibrium solutions, the disappearance of permafrost based on their metrics does not necessarily mean that deep permafrost will have completely degraded from that area at the time of diagnosis; it only means that permafrost is no longer sustainable under those climatic conditions. These methods have been used to make inferences about near-surface permafrost [*Anisimov and Nelson*, 1996], but they are underpinned by steady-state assumptions.

The winter period for computing snow depth is defined as the time during which air temperature is below 0°C. Consequently, as temperatures warm, the length of the snow season also becomes shorter. While the annual temperature cycle is sinusoidal, snow depth is seasonally asymmetric due to the accumulation process. To obtain a meaningful average snow depth that reflects its impact as ground insulation we weight the depth of snow for each month by the degree to which the temperature that month is below freezing. That is, for all months (i) with temperature (T) below freezing for the water year October to September, mean snow depth (D) is given as:

$$\overline{D} = \sum_i \left(\frac{D_i \times T_i}{\sum_i T_i} \right) \quad \text{for} \quad T_i < 0°\text{C} \tag{1}$$

Each month snow water equivalent (SWE) and snow depth were used to compute snow density, which is needed for estimating snow thermal conductivity. The mean winter density was weighted in the same way as depth. All CMIP5 models provide SWE data, while some (e.g. CSIRO and HadGEM2) omit snow depth, in which case a snow density

of 250kg m^{-3} was used for conversion. The CFSRR snow depth is an analyzed field but uses an unrealistic constant density of 100 kg m^{-3} so we again applied 250kg m^{-3}.

3.2.1 Surface Frost Index (SFI)

The Surface Frost Index (SFI) as described by *Nelson and Outcalt* [1987] is a climate based index:

$$SFI = \frac{\sqrt{DDF^*}}{\sqrt{DDF^*}+\sqrt{DDT}} \quad (2)$$

Where *DDF** is the sum of freezing degree days modified for snow insulation and *DDT* is the sum of thawing degree days computed from the sinusoidal climate. It uses no information about the surface state (soils, vegetation etc.) but provides an idea of where the climate would be conducive to the existence of permafrost. The only departure we make from the original SFI method is the computation of mean winter snow depth as given above. Thermal conductivity and heat capacity of snow is computed as per the original paper as a function of density. The SFI ranges from 0.0 to 1.0, with values of 0.5 – 0.6 indicating sporadic permafrost, 0.60–0.67 indicating extensive (akin to discontinuous) permafrost and values above 0.67 are taken as continuous permafrost.

3.2.2 Kudryavtsev Method (KUD)

The Kudryavtsev Method (KUD; *Kudyavtsev et al.*, [1974]) is an analytic model that produces a steady state (equilibrium) solution under the assumption of constant sinusoidal air temperature forcing with a mean winter snow cover and damping from organic matter or vegetation. Theoretical derivation of the model is given in *Yershov* [1998; Chapter 1] with an additional excellent description available in *Sazonova and Romanovsky* [2003] and *Romanovsky and Osterkamp* [1997]. This method also forms the basis for the State Hydrometeorological Institute (SHI) permafrost model [*Anisimov et al.*, 1997].

The required spatially explicit mineral soil textures (% sand, silt and clay) are taken from [*Zobler*, 1986] and computation of thermal properties follow *Farouki* [1981]. Soil saturations are derived as a function of the WATCH soil moisture estimates [*Harding et al.*, 2011] and are kept constant. Excess soil ice is not accounted for, nor is the impact of ground subsidence.

The thickness of the organic mat (considered a combination of organic material in the soil, mosses and ground cover vegetation) was assumed to be a maximum of 75cm and scaled to the density of soil organic matter distribution given in the *Global Soil Data Task* [2000]; hence over most of the Arctic permafrost region the prescribed organic mat is 10-25cm thick. Thermal diffusivity of the organic mat under both frozen and thawed conditions is somewhat subjective as it is dependent upon its composition, but we follow the values used by *Anisimov et al.* [1997]. The KUD model has two primary outputs; active layer thickness and the mean annual temperature at the top of the permafrost,

which can be used to indicate if permafrost is sustainable. When forced with reanalysis data we produce permafrost temperatures in eastern Siberia similar to those in *Sazonova and Romanovsky*, [2003].

4 Analysis of Permafrost in CMIP5 Models

4.1 Climate of the Present-day Permafrost Region

The two most important climatic variables for permafrost are air temperature and snow depth. We use the reference period of 1986-2005 to perform a climate evaluation over the area where the IPA map suggests that continuous and discontinuous permafrost exists. Data was interpolated to the CCSM4 grid and all averages are area weighted.

Climate means are given in Table 1, but in Figure 3 we use the mean of the four reanalysis products as a reference and show departures for each model. Eight out of 17 models with data for this period have a cold bias of 0.5°C or more, with five having a 2°C or colder bias. Only 3 models have a warm bias of 0.5°C or more (Figure 3a). When viewed in terms of seasonality (Figure 3b, c), the majority of the discrepancy between the models and the reanalyses occurs in the cold winter months and fits with the difficulty models have in modeling stable boundary layer conditions [ECMWF-GABLS, 2011]. The range of mean annual minimum temperature averaged over the permafrost domain is greater than 10°C across the CMIP5 models, while their mean annual maximum only spans 5°C. The reanalyses also display a greater range in winter. BCC-CSM1-1, CSIRO,

293 the Hadley models, and NorESM1-M all have cold biases throughout the year while
294 CanESM2, MIROC5 and MIROC-ESM are warmer throughout the year. For normalized
295 winter snow depths (Figure 3d), the reanalyses lack agreement despite two of them
296 (ERA-I and CFSRR) being analyzed (assimilated) fields; however, their mean provides a
297 reference. Ten of the models have an absolute anomaly of 0.05m or more and most
298 models have too little snow compared to the reference. CCSM4 and NorESM1-M (which
299 includes the atmosphere and land components from CCSM4) show a high snow bias
300 which degrades the skill of modeling permafrost, particularly in certain regions (see
301 *Lawrence et al.*, [2012]). The same problem afflicts BCC-CSM1-1. A normalized snow
302 depth anomaly of 0.1m will impact ground temperatures given that much of the Arctic
303 and Tibet have *peak* snow depths of less than 0.5m [*Brown and Brasnett*, 2010] and
304 importantly, the ability of snow to insulate the ground from cold winter temperatures is
305 non-linear at shallow depths [*Zhang*, 2005; *Lawrence and Slater*, 2010].
306
307
308 ## 4.2 Simulation of Present and Future Permafrost by CMIP5 Models
309
310 For the 13 models that provided soil temperatures, we compare the range of permafrost
311 areas diagnosed via both TSL and SFI for 1900-2099 (using *r1i1p1*; Figure 4a) under
312 RCP8.5. In six of the 13 instances, SFI gives greater starting (1900) and ending (2099)
313 area, four instances do the opposite with TSL having greater area, two instances where
314 TSL is within the bounds of SFI and one where TSL and SFI have the same minimum but
315 TSL had a larger maximum. As defined by TSL, the ability of many CMIP5 models to

316 directly simulate permafrost is quite poor. For example, across the 13 CMIP5 models in
317 Figure 4a, the range of maximum permafrost areas since 1900 via TSL is 5 to 27 $\times 10^6$
318 km^2. In contrast, this range is only half as large via SFI at 11 to 21×10^6 km^2. The fact that
319 TSL produces both larger and smaller permafrost areas than respective SFI results
320 suggests that the land models cause more to the overall range of results than do climate
321 discrepancies, for example compare the results of the BCC-CSM1-1 and GFDL models
322 in Figure 4a. Compared to IPA map observations, all CMIP5 model climates
323 overestimate permafrost area on the Tibetan Plateau via SFI and KUD for 1986-2005 and
324 all but two models overestimate this area using the TSL diagnostic (not shown). Based on
325 the IPA map, the Tibetan Plateau contains less than 7% of northern hemisphere
326 continuous + discontinuous permafrost area (but more recent data suggests discontinuous
327 permafrost may be slightly more prevalent [*Yang et al.*, 2010]). Permafrost changes in
328 the Arctic are therefore of greater consequence to the global climate.
329
330 Recall that the large variation in permafrost extent computed by TSL across the CMIP5
331 models is a function of both climate and land model differences while SFI differences are
332 driven purely by climate differences. The disparity in permafrost extent between the two
333 methods therefore suggests that with regard to assessing permafrost, the role of the land
334 surface model can be as significant as that of the CGCM's simulated surface climate. The
335 relationship between the influences of climate compared to the land model can be seen in
336 Figure 4b where we show SFI area against TSL area for each year and for each model.
337 Note that time is *not* an axis in Figure 4b, but permafrost area decreases over time with
338 warming (in general for each model/scenario, time can be thought of as running along

each line from upper right to lower left). Further, we emphasize that this is a comparative analysis and the ideal trajectory within this two model space is unknown. Nonetheless several points can be inferred from this figure. Firstly, the influence of climate biases is demonstrated by the large range of SFI permafrost area for the year 2000 (10.5 – 19.5×10^6 km^2, shown by dots in Figure 4b) compared to the observed area of about 16×10^6 km^2. Secondly, where permafrost area is greater than 2×10^6 km^2 for either method, there is a very linear relationship between SFI and TSL areas. Below 2×10^6 km^2 non-linear behavior occurs as permafrost persists only in extremely cold regions or may cross thresholds in the models as warming becomes greater. Thirdly, despite the differences in climate trajectories between various RCP's, the SFI to TSL relationship remains similar for individual models. The linear relation prompts us to examine the sensitivity of permafrost to temperature change over the permafrost region (Section 4.2.2), while the consistent differences between permafrost area as diagnosed by TSL and SFI prompts inquiry into the influence of the land model physics relative to the surface climate simulation (Section 4.2.1).

4.2.1 Impact of the Land Surface Model

CMIP5 models with their trace well above the 1:1 line in Figure 4b (e.g. GFDL-ESM2M, HadGEM2, MIROC) can be considered to have land models that produce "colder" soils in frost prone regions and the reverse is true for models that sit below 1:1 in Figure 4b (e.g. BCC-CSM1-1, CanESM2, GISS-ES-R, MPI-ESM-LR). Note that the 1:1 line is only a reference point, not truth nor observation. Models that start their trace to the left

side of the diagram (i.e. have low SFI values) have warmer, less permafrost prone, climates (e.g. CanESM2). The MIROC models are subject to having both a "colder" land model and a warm climate. The ideal position for a model on Figure 4b is unknown as SFI is simply another model, but one that acts as a climate normalizing agent.

In several instances, the same land model is applied in slightly different CMIP5 models e.g. CCSM4 and NorESM1-M both use CLM4, the HadGEM2 models both use MOSES2.2 and the MIROC models share the same scheme (see Table 1). While the climate of these models can be different (see Figure 3), the behavior of each pair in Figure 4b is similar, thus indicating good discrimination of land model influence (e.g., the HadGEM2 models practically overlie each other, as do CCSM4 and NorESM1-M). The MIROC models both show an accelerated decline in TSL area once SFI estimates are 2.5×10^6 km^2 or less, suggesting that this more frost-prone land model finally succumbs to the warming climate, possibly crossing a threshold of sorts. MIROC5 runs at twice the resolution of MIROC-ESM, which may partly explain their different positions, but their behavior is similar.

According to the classification of *Slater et al.*, [2001], the MOSES2.2 land model (HadGEM2; *Essery et al.*, [2001]) has an implicit snow scheme which effectively negate or reduce the insulating capacity of snow. That is, the top soil layer in this model takes on the same temperature of the air-snow interface. Consequently, the soils tend to be too cold. A complimentary study to this one by [*Koven et al.*, 2013] demonstrates this problem quite well. Despite the high resolution soil column in GFDL's land model LM3

385 (20 layers, with 15 layers in the top 3m; Figure 2) and the use of a multi-layer snow
386 model, it shows a structural deficiency of minimal snow insulation, causing it to have
387 very cold soil temperatures (not shown) and to simulate excessive permafrost. Another
388 example of model structure heavily impacting the embedded permafrost simulation is the
389 CanESM2 model, which uses the three soil layer CLASS land model [*Verseghy*, 2000],
390 the third layer spanning 0.35-4.10m depth (Figure 2). Due to its shallow upper bound and
391 low latent heat sink (maximum total frozen soil moisture content is below 150mm for
392 much of the permafrost region due to imposition of bedrock), this layer is subject to large
393 annual temperature fluctuations, thus it tends not to stay frozen throughout the year in
394 more marginal permafrost zone climates. Permafrost area via annual mean soil
395 temperature (MST) in CanESM2 gives a mean area of 20.8×10^6 km^2 for 1986-2005
396 (compared to 3.75×10^6 km^2 via TSL), but by 2099 under RCP8.5, MST permafrost area
397 is down to 2.9×10^6 km^2. The MPI-EMS-LR land model does not include explicit soil
398 freezing processes [*Roeckner et al.*, 2003], thus has large seasonal soil temperature
399 amplitudes which explains the large MST (22.7×10^6 km^2, 1986-2005) area compared to
400 TSL (10.1×10^6 km^2, 1986-2005). Improved process representation can also be detected,
401 For example, BCC-CSM1-1 uses BCC_AVIM1 as its land model, which includes neither
402 organic soil matter nor a deep soil column. BCC_AVIM1, which uses a 10-layer soil
403 column based on the old CLM3 model [*Oleson et al.*, 2004], thus maintains less
404 permafrost than CLM4 (used by CCSM4) [*Lawrence et al.*, 2008, 2012] resulting in
405 BCC-CSM-1 having a lower ratio of TSL:SFI permafrost area than CCSM4 (Figure 4b).
406

4.2.2 Permafrost Climate Sensitivity

For each CMIP5 model in Figure 4, respective change in air temperature over the present day permafrost region (Figure 1) was regressed against the change in permafrost area for instances where permafrost area was greater than 2×10^6 km^2. Permafrost area was computed via TSL, SFI and KUD methods for all RCPs. The linearity of this relationship is shown in Figure 5; similar linear relations have been found for sea ice [*Mahlstein and Knutti*, 2012]. Across all 13 CMIP5 models for each of TSL, SFI and KUD, the mean coefficient of determination (R^2) of the linear regressions is above 0.80, 0.85, 0.91 and 0.94 for RCP2.6, RCP4.5, RCP6.0 and RCP8.5 respectively, suggesting a good linear fit. The fit becomes better with higher RCP's as interannual to decadal scale variability has less influence relative to the warming signal, but there is considerable variability in the sensitivity of the models (see Table 2). For example, the TSL sensitivity of INMCM4 is a notable outlier at only 0.75×10^6 km^2/°C. For all three methods (TSL, SFI and KUD), the mean sensitivity decreases by about 0.15×10^6 km^2/°C from RCP2.6 to RCP8.5, as very cold regions with more resilient permafrost slowly become subject to degradation under RCP8.5. Of interest is that models with widely different TSL estimates of permafrost can have similar sensitivities. For example, in RCP8.5 the sensitivities of GFDL-ESM2M and MPI-ESM-LR are 1.7 and 1.75×10^6 km^2/°C respectively despite GDLF-ESM2M having more permafrost in 2099 than MPI-ESM-LR has in 1900.

It is important to be aware that such regression analysis is purely empirical and the sensitivities do not apply on a regional basis. Indeed, the SFI and KUD cases show that

different climate trajectories applied to a fixed model can produce a variety of sensitivities therefore suggesting that spatial and temporal differences in climate change (e.g., seasonal differences, differences in polar amplification, snow change regionality) can play an important role in determining how fast permafrost degrades. The variance of sensitivity across the models is greater under TSL than SFI or KUD which is perhaps not surprising given the added degrees of freedom that the prognostic land models generate in the TSL method. The higher sensitivity of KUD compared to SFI may partly stem from the fact that it overestimates permafrost area in marginal regions, thus permafrost retreats rapidly in places. The KUD method has been typically applied to colder, continuous permafrost regions;

The metric "percentage change in permafrost area" has been used to make comparisons between modeling studies [*Saito et al.*, 2007; *Zhang et al.*, 2008; *Dankers et al.*, 2011], but results presented here suggest it is not very informative for comparing future states because the sensitivity of permafrost area to warming can be quite similar while the absolute areas and percentage changes are quite different.

5 Future Projections Based on Climate Change

Climate biases presented in Figure 3, along with the spread of permafrost area shown in Figure 4 and the sensitivity analysis in Figure 5, suggest that an assessment of future permafrost might be more informative when performed with respect to climatic change rather than by raw diagnosis from CMIP5 models. Issues such as inherent climate biases

453 can be ameliorated through this approach but uncertainty will remain as some models
454 clearly perform better than others across a range of diagnostics.
455
456 Figure 6 gives an indication of the mean trend and projected change in temperature over
457 the present-day permafrost region (Figure 1). For each CMIP5 model and reanalysis, the
458 average temperature over the region is computed and their respective 1986-2005 average
459 is subtracted. Despite the absolute climate biases in individual models (Figure 3) the rate
460 of change over the last 25 years (0.46°C/decade based on the reanalysis data) is captured
461 very well by the mean of CMIP5 models. The mean temperature change by 2099 across
462 available models is 2.2°C, 3.8°C, 4.5°C and 7.8°C for RCP2.6, RCP4.5, RCP6.0 and
463 RCP8.5, but there is a large range across the models, for example, HadGEM2-ES warms
464 +6.2°C (+11.3°C) while GISS-E2-R only warms by +1.7°C (+4.6°C) for RCP4.5
465 (RCP8.5).
466
467 To project permafrost on the basis of climate change we can apply the SFI or KUD
468 methods, remembering though that they showed a ~25-38% greater sensitivity than TSL.
469 To create forcing data sets we take an average of the four reanalysis products for both air
470 temperature and snow depth over 1986-2005, then for each CMIP5 model and RCP, at
471 each grid box, the temperature change and a proportional change in snow from this time
472 period is added to the reanalysis mean to form trajectories of future climate.
473 Unfortunately this method does not account for the fact that biases can (and do) change
474 over time. Fifteen models provided required temperature *and* snow data for RCP4.5 and
475 RCP8.5 while only ten had data for RCP2.6 and nine for RCP6.0.

For projecting future permafrost under these trajectories, the SFI area has been tuned to match observed area during the reanalysis forced period by using a minimum frost index value of 0.58, rather than the 0.60 suggested by *Nelson and Outcalt*, [1987]. Given the range of warming per scenario and the different sensitivities caused by alternate climate evolution it is not surprising to see sizable variance for each RCP projection of permafrost area (Figure 7). Mean values of near-surface permafrost area (recall that the SFI method tells us the permafrost suitability area under climate equilibrium, not the actual permafrost area at 2099) by 2099 are 10.0, 7.5, 5.9 and 2.1×10^{6} km^{2} for RCP2.6, RCP4.5, RCP6.0 and RCP8.5 respectively. While the areas suitable for permafrost in RCP2.6 and RCP4.5 appear to have stabilized by 2099, RCP6.0 and RCP8.5 are still on a declining trajectory.

Areas of sustainable near-surface permafrost by the year 2099 for all RCPs are given in Figure 8 which shows the number of climate trajectories (one trajectory per CGCM) that retain permafrost for a given location. Under RCP2.6 the majority of present day continuous permafrost is likely to remain with some transforming to discontinuous. The increased warming of RCP4.5 and RCP6.0 see permafrost retreat further north with Alaska showing vulnerability to degradation. RCP8.5 sees a wide span in expectations with a couple of cooler models keeping permafrost over large portions of Eurasia and Canada while others remove virtually all permafrost (which is not surprising given 11°C warming). However, the Canadian Archipelago, eastern Siberian uplands, high Arctic coastal Russia (e.g. the Taymir Peninsula) and parts of Tibet are likely to sustain

permafrost even under the large warming of RCP8.5. The vast majority (80%) of available climate change trajectories return respective sustainable permafrost areas of less than 9.6×10^6 km^2 (RCP4.5) and 3.5×10^6 km^2 (RCP8.5) via SFI by 2099 (shown by the dark red pixels in Figure 8). Hence, we take these to represent conservative estimates of future permafrost.

6 Summary and Conclusion

We have applied several methods of diagnosing permafrost over a range of climate models and future scenarios of climate change. From this analysis a number of salient points have become apparent and these are summarized here.

Permafrost relevant climate bias in temperatures or snow accumulation over the present-day permafrost region can be significant when compared to reanalyses for the 1986-2005 period. Impacts of biases are particularly evident from the large range in permafrost area diagnosed using only climate indices of each model (e.g. the SFI method). Models display a greater range of temperature biases during the winter period and shallow Arctic snow depths mean that small differences (e.g. 10cm) seen in average snow depth will impact insulating abilities.

The range of permafrost area directly diagnosed from modeled soil temperatures (TSL) is extremely large (~4 to 25×10^6 km^2 averaged over 1986-2005) and the range in mean soil temperature (MST; Table 1) over the present day permafrost region for 1986-2005 is over

522 7°C across the models. Hence, it can be concluded that in general permafrost is not well
523 represented by the ensemble of CMIP5 models, though not all models perform poorly.
524 These large ranges are due to two factors: (a) differences in simulated surface climate
525 and (b) varying abilities of the underlying land surface models, with the latter likely
526 having a larger impact (Figure 4a, Section 4.2). When TSL is compared to climate-based
527 permafrost indices such as the surface frost index (SFI) we see that some land models are
528 particularly prone to producing cold soils with large permafrost areas while others
529 encourage thawing in the upper levels of the soil. The comparison of TSL to SFI exposes
530 weaknesses in many model's representation of permafrost processes. The structure of the
531 land model, for example the insulating ability of its snow scheme or the discretization of
532 the soil column, can play a significant role in the determining of permafrost extent.
533 Similar behavior is seen across all RCP scenarios for each individual CMIP5 model when
534 comparing change in permafrost area via TSL and SFI indicating that land model
535 responses are consistent regardless of climate trajectory.
536
537 Despite large differences in the absolute permafrost area, the relationship between the
538 decrease in permafrost area and the warming air temperature over the present-day
539 permafrost region can be similar between many models and is approximately linear for
540 all models. Spatial and temporal differences in the pattern of climate change can impact
541 this permafrost-climate sensitivity as evidenced by the spectrum of sensitivity under
542 either the SFI or KUD models. Averaged across all methods and models under RCP8.5,
543 permafrost area sensitivity is 1.67×10^{6} km^2/°C but the sensitivity spans a wide range
544 ($0.75 - 2.32\times10^{6}$ km^2/°C).

Using projected change in climate relative to present-day climate (i.e., bias corrected climate trajectories rather than absolute climate trajectories direct from the CGCMs) we have estimated potential trajectories for sustainable near-surface permafrost out to 2099. When measured over the present-day permafrost region, the range of warming for a given century-scale RCP scenario across all CMIP5 models can be as large as the average warming, resulting in quite different permafrost regimes by the end of the 21st century. Nonetheless, robust results of future permafrost sustainability are evident, particularly in the core CMIP5 experiments. Conservatively, under RCP4.5 near-surface permafrost is unlikely to be sustainable in the present day discontinuous zone and under RCP8.5 existence will be reduced to the Canadian Archipelago, Russian Arctic coast and East Siberian uplands. Projections based on SFI or KUD provide useful insights to future permafrost distribution but it is preferable for Earth system models to include the full physics of subsurface processes in order to allow for interactions with hydrology, vegetation and biogeochemical cycling and thus correctly account for, and quantify, feedbacks related to permafrost degradation on the local and global climate system.

7 Acknowledgements

Support from NSF via ARC-1041081, ARC-0902057, ARC-0901962 is gratefully acknowledged. This research was also supported by funding from the US Department of Energy, Office of Biological and Environmental Research, as part of its Climate Change Prediction Program, cooperative agreement no. DE-FC03-97ER62402/A010. Thanks to

Charlie Koven for useful discussions, the CMIP5 model groups for their data, model developers for information about model structures and three anonymous reviewers for aiding clarity.

8 References

Akerman, H. J., and M. Johansson (2008), Thawing permafrost and thicker active layers in sub-arctic Sweden, *PERMAFROST AND PERIGLACIAL PROCESSES*, *19*(3), 279–292, doi:10.1002/ppp.626.

Anisimov, O., and F. Nelson (1996), Permafrost distribution in the Northern Hemisphere under scenarios of climatic change, *GLOBAL AND PLANETARY CHANGE*, *14*(1-2), 59–72, doi:10.1016/0921-8181(96)00002-1.

Anisimov, O., N. Shiklomanov, and F. Nelson (1997), Global warming and active-layer thickness: results from transient general circulation models, *GLOBAL AND PLANETARY CHANGE*, *15*(3-4), 61–77, doi:10.1016/S0921-8181(97)00009-X.

BCC (2012), *Beijing Climate Center, Climate System Model*. [online] Available from: http://bcc.cma.gov.cn/bcccsm/web/channel-42.htm

Boone, A., V. Masson, T. Meyers, and J. Noilhan (2000), The influence of the inclusion of soil freezing on simulations by a soil-vegetation-atmosphere transfer scheme, *Journal of Applied Meteorology*, *39*(9), 1544–1569, doi:10.1175/1520-0450(2000)039<1544:TIOTIO>2.0.CO;2.

Brown, R., and B. Brasnett (2010), Canadian Meteorological Centre (CMC) Daily Snow Depth Analysis Data. © Environment Canada, 2010. Boulder, Colorado USA: National Snow and Ice Data Center. Digital media, [online] Available from: http://nsidc.org/data/NSIDC-0447.html

Cheng, G., and T. Wu (2007), Responses of permafrost to climate change and their environmental significance, Qinghai-Tibet Plateau, *JOURNAL OF GEOPHYSICAL RESEARCH-EARTH SURFACE*, *112*(F2), doi:10.1029/2006JF000631.

Christensen, T., T. Johansson, H. Akerman, M. Mastepanov, N. Malmer, T. Friborg, P. Crill, and B. Svensson (2004), Thawing sub-arctic permafrost: Effects on vegetation and methane emissions, *GEOPHYSICAL RESEARCH LETTERS*, *31*(4), doi:10.1029/2003GL018680.

Clark, D., I. Stirling, and W. Calvert (1997), Distribution, characteristics, and use of earth dens and related excavations by polar bears on the Western Hudson Bay lowlands, *ARCTIC*, *50*(2), 158–166.

Dankers, R., E. J. Burke, and J. Price (2011), Simulation of permafrost and seasonal thaw depth in the JULES land surface scheme, *The Cryosphere*, *5*(3), 773–790, doi:10.5194/tc-5-773-2011.

Dee, D. P. et al. (2011), The ERA-Interim reanalysis: configuration and performance of the data assimilation system, *QUARTERLY JOURNAL OF THE ROYAL METEOROLOGICAL SOCIETY*, *137*(656, Part a), 553–597, doi:10.1002/qj.828.

Dunne, J. P. et al. (2012), GFDL's ESM2 Global Coupled Climate-Carbon Earth System Models. Part I: Physical Formulation and Baseline Simulation Characteristics, *JOURNAL OF CLIMATE*, *25*(19), 6646–6665, doi:10.1175/JCLI-D-11-00560.1.

Ek, M. B., K. E. Mitchell, Y. Lin, E. Rogers, P. Grunmann, V. Koren, G. Gayno, and J. D. Tarpley (2003), Implementation of Noah land surface model advances in the National Centers for Environmental Prediction operational mesoscale Eta model, *Journal of Geophysical Research-Atmospheres*, *108*(D22), doi:10.1029/2002JD003296.

Essery, R. L. H., M. J. Best, and P. M. Cox (2001), *MOSES 2.2 Technical Documentation*, Hadley Centre technical note 30. [online] Available from: http://www.metoffice.gov.uk/media/pdf/9/j/HCTN_30.pdf

Fortier, D., M. Allard, and Y. Shur (2007), Observation of rapid drainage system development by thermal erosion of ice wedges on Bylot island, Canadian Arctic Archipelago, *PERMAFROST AND PERIGLACIAL PROCESSES*, *18*(3), 229–243, doi:10.1002/ppp.595.

Gordon, H. B., L. D. Rotstayn, J. L. McGregor, M. R. Dix, E. A. Kowalczyk, S. O'Farrell, and et al. (2002), *The CSIRO Mk3 Climate System Model*.

Harding, R. et al. (2011), WATCH: Current Knowledge of the Terrestrial Global Water Cycle, *JOURNAL OF HYDROMETEOROLOGY*, *12*(6), 1149–1156, doi:10.1175/JHM-D-11-024.1.

Ji, J. (1995), A climate-vegetation interaction model: simulating physical and biological processes at the surface, *J. Biogeography*, *22*, 2063–2069.

Jorgenson, M., Y. Shur, and E. Pullman (2006), Abrupt increase in permafrost degradation in Arctic Alaska, *GEOPHYSICAL RESEARCH LETTERS*, *33*(2), doi:10.1029/2005GL024960.

Koster, R., M. Suarez, A. Ducharne, M. Stieglitz, and P. Kumar (2000), A catchment-based approach to modeling land surface processes in a general circulation model

638 1. Model structure, *JOURNAL OF GEOPHYSICAL RESEARCH-*
639 *ATMOSPHERES*, *105*(D20), 24809–24822, doi:10.1029/2000JD900327.

640 Koven, C., W. Riley, and A. Stern (2013), Analysis of permafrost thermal dynamics and
641 response to climate change in the CMIP5 Earth System Models, *Journal of*
642 *Climate*, doi:10.1175/JCLI-D-12-00228.1.

643 Larsen, P. H., S. Goldsmith, O. Smith, M. L. Wilson, K. Strzepek, P. Chinowsky, and B.
644 Saylor (2008), Estimating future costs for Alaska public infrastructure at risk from
645 climate change, *GLOBAL ENVIRONMENTAL CHANGE-HUMAN AND POLICY*
646 *DIMENSIONS*, *18*(3, SI), 442–457, doi:10.1016/j.gloenvcha.2008.03.005.

647 Lawrence, D., and A. Slater (2005), A projection of severe near-surface permafrost
648 degradation during the 21st century, *GEOPHYSICAL RESEARCH LETTERS*,
649 *32*(24), doi:10.1029/2005GL025080.

650 Lawrence, D. M., and A. G. Slater (2010), The contribution of snow condition trends to
651 future ground climate, *CLIMATE DYNAMICS*, *34*(7-8), 969–981,
652 doi:10.1007/s00382-009-0537-4.

653 Lawrence, D. M., A. G. Slater, V. E. Romanovsky, and D. J. Nicolsky (2008), Sensitivity
654 of a model projection of near-surface permafrost degradation to soil column depth
655 and representation of soil organic matter, *JOURNAL OF GEOPHYSICAL*
656 *RESEARCH-EARTH SURFACE*, *113*(F2), doi:10.1029/2007JF000883.

657 Lawrence, D. M. et al. (2011), Parameterization Improvements and Functional and
658 Structural Advances in Version 4 of the Community Land Model, *JOURNAL OF*
659 *ADVANCES IN MODELING EARTH SYSTEMS*, *3*, doi:10.1029/2011MS000045.

660 Lawrence, D. M., A. G. Slater, and S. C. Swenson (2012), Simulation of Present-Day and
661 Future Permafrost and Seasonally Frozen Ground Conditions in CCSM4, *Journal*
662 *of Climate*, *25*(7), 2207–2225, doi:10.1175/JCLI-D-11-00334.1.

663 LeMoigne, P., A. Boone, J. Mahfouf, B. van den Hurk, J. Noilhan, and 10 others (2009),
664 *SURFEX Scientific Documentation*. [online] Available from:
665 http://www.cnrm.meteo.fr/surfex/IMG/pdf/surfex_scientific_documentation.pdf

666 Lloyd, A., K. Yoshikawa, C. Fastie, L. Hinzman, and M. Fraver (2003), Effects of
667 permafrost degradation on woody vegetation at arctic treeline on the Seward
668 Peninsula, Alaska, *PERMAFROST AND PERIGLACIAL PROCESSES*, *14*(2), 93–
669 101, doi:10.1002/ppp.446.

670 Mahlstein, I., and R. Knutti (2012), September Arctic sea ice predicted to disappear near
671 2°C global warming above present, *J. Geophys. Res.*, *117*, 11 PP.,
672 doi:201210.1029/2011JD016709.

673 Nelson, F., and S. Outcalt (1987), A Computational Method for Prediction and
674 Regionalization of Permafrost, *Arctic and Alpine Research*, *19*(3), 279–288,
675 doi:10.2307/1551363.

676 Oleson, K. W., D. Yonhjui, G. B. Bonan, and et al. (2004), *Technical description of the*
677 *Community Land Model CLM3.0*, NCAR Tech. Note NCAR/TN-461+STR.
678 [online] Available from:
679 http://www.cgd.ucar.edu/tss/clm/distribution/clm3.0/index.html

680 Oleson, K. W., D. M. Lawrence, G. B. Bonan, M. G. Flanner, E. Kluzek, P. J. Lawrence,
681 S. Levis, S. C. Swenson, P. E. Thornton, and et al (2010), *Technical Description*
682 *of version 4.0 of the Community Land Model (CLM)*, NCAR Technical Note
683 NCAR/TN-478+STR. [online] Available from:
684 http://www.cesm.ucar.edu/models/clm/

685 Onogi, K. et al. (2007), The JRA-25 reanalysis, *JOURNAL OF THE*
686 *METEOROLOGICAL SOCIETY OF JAPAN*, *85*(3), 369–432,
687 doi:10.2151/jmsj.85.369.

688 Rienecker, M. M. et al. (2011), MERRA: NASA's Modern-Era Retrospective Analysis
689 for Research and Applications, *JOURNAL OF CLIMATE*, *24*(14), 3624–3648,
690 doi:10.1175/JCLI-D-11-00015.1.

691 Roeckner, E. et al. (2003), *The Atmospheric General Circulation Model ECHAM5; Part*
692 *1 Model Description*, MPI Report No. 349, Max Planck Institute, Hamburg.

693 Romanovsky, V., and T. Osterkamp (1997), Thawing of the active layer on the coastal
694 plain of the Alaskan Arctic, *PERMAFROST AND PERIGLACIAL PROCESSES*,
695 *8*(1), 1–22.

696 Romanovsky, V. E., S. L. Smith, and H. H. Christiansen (2010), Permafrost Thermal
697 State in the Polar Northern Hemisphere during the International Polar Year 2007-
698 2009: a Synthesis, *PERMAFROST AND PERIGLACIAL PROCESSES*, *21*(2, SI),
699 106–116, doi:10.1002/ppp.689.

700 Rosenzweig, C., and F. Abramopoulos (1997), Land-surface model development for the
701 GISS GCM, *Journal of Climate*, *10*(8), 2040–2054, doi:10.1175/1520-
702 0442(1997)010<2040:LSMDFT>2.0.CO;2.

703 Rouse, W. et al. (1997), Effects of climate change on the freshwaters of arctic and
704 subarctic North America, *HYDROLOGICAL PROCESSES*, *11*(8), 873–902,
705 doi:10.1002/(SICI)1099-1085(19970630)11:8<873::AID-HYP510>3.0.CO;2-6.

706 Saha, S. et al. (2010), THE NCEP CLIMATE FORECAST SYSTEM REANALYSIS,
707 *BULLETIN OF THE AMERICAN METEOROLOGICAL SOCIETY*, *91*(8), 1015–
708 1057, doi:10.1175/2010BAMS3001.1.

709 Saito, K., M. Kimoto, T. Zhang, K. Takata, and S. Emori (2007), Evaluating a high-
710 resolution climate model: Simulated hydrothermal regimes in frozen ground
711 regions and their change under the global warming scenario, *JOURNAL OF*
712 *GEOPHYSICAL RESEARCH-EARTH SURFACE*, *112*(F2),
713 doi:10.1029/2006JF000577.

714 Sato, N., P. Sellers, D. Randall, E. Schneider, J. Shukla, J. Kinter, Y. Hou, and E.
715 Albertazzi (1989), Effects of Implementing the Simple Biosphere Model in a
716 General-Circulation Model, *Journal of the Atmospheric Sciences*, *46*(18), 2757–
717 2782, doi:10.1175/1520-0469(1989)046<2757:EOITSB>2.0.CO;2.

718 Sazonova, T., and V. Romanovsky (2003), A model for regional-scale estimation of
719 temporal and spatial variability of active layer thickness and mean annual ground
720 temperatures, *PERMAFROST AND PERIGLACIAL PROCESSES*, *14*(2), 125–
721 139, doi:10.1002/ppp.449.

722 Schuur, E. A. G. et al. (2008), Vulnerability of permafrost carbon to climate change:
723 Implications for the global carbon cycle, *BIOSCIENCE*, *58*(8), 701–714,
724 doi:10.1641/B580807.

725 Schuur, E. A. G., J. G. Vogel, K. G. Crummer, H. Lee, J. O. Sickman, and T. E.
726 Osterkamp (2009), The effect of permafrost thaw on old carbon release and net
727 carbon exchange from tundra, *NATURE*, *459*(7246), 556–559,
728 doi:10.1038/nature08031.

729 Sellers, P., Y. Mintz, Y. Sud, and A. Dalcher (1986), A Simple Biosphere Model (SiB) fo
730 use within General-Circulation Models, *Journal of Atmospheric Sciences*, *43*(6),
731 505–531, doi:10.1175/1520-0469(1986)043<0505:ASBMFU>2.0.CO;2.

732 Slater, A. et al. (2001), The representation of snow in land surface schemes: Results from
733 PILPS 2(d), *JOURNAL OF HYDROMETEOROLOGY*, *2*(1), 7–25,
734 doi:10.1175/1525-7541(2001)002<0007:TROSIL>2.0.CO;2.

735 Smith, L., Y. Sheng, G. MacDonald, and L. Hinzman (2005), Disappearing Arctic lakes,
736 *SCIENCE*, *308*(5727), 1429, doi:10.1126/science.1108142.

737 Stendel, M., and J. Christensen (2002), Impact of global warming on permafrost
738 conditions in a coupled GCM, *GEOPHYSICAL RESEARCH LETTERS*, *29*(13),
739 doi:10.1029/2001GL014345.

740 Takata, K., S. Emori, and T. Watanabe (2003), Development of the minimal advanced
741 treatments of surface interaction and runoff, *Global and Planetary Change*,
742 *38*(1-2), 209–222, doi:10.1016/S0921-8181(03)00030-4.

743 Thibault, S., and S. Payette (2009), Recent Permafrost Degradation in Bogs of the James
744 Bay Area, Northern Quebec, Canada, *PERMAFROST AND PERIGLACIAL*
745 *PROCESSES*, *20*(4), 383–389, doi:10.1002/ppp.660.

746 Verseghy, D. (2000), The Canadian Land Surface Scheme (CLASS): Its history and
747 future, *ATMOSPHERE-OCEAN*, *38*(1), 1–13.

748 Viterbo, P., A. Beljaars, J. Mahfouf, and J. Teixeira (1999), The representation of soil
749 moisture freezing and its impact on the stable boundary layer, *QUARTERLY*
750 *JOURNAL OF THE ROYAL METEOROLOGICAL SOCIETY*, *125*(559, Part a),
751 2401–2426, doi:10.1256/smsqj.55903.

752 Volodin, E. M., and V. N. Lykosov (1998a), Parametrization of heat and moisture
753 transfer in the soil-vegetation system for use in atmospheric general circulation
754 models: 1. Formulation and simulations based on local observational data,
755 *Izvestiya Akademii Nauk Fizika Atmosfery I Okeana*, *34*(4), 453–465.

756 Volodin, E. M., and V. N. Lykosov (1998b), Parametrization of heat and moisture
757 transfer in the soil-vegetation system for use in atmospheric general circulation
758 models: 2. Numerical experiments on climate modeling, *Izvestiya Akademii*
759 *Nauk Fizika Atmosfery I Okeana*, *34*(5), 622–633.

760 Wrona, F. J., T. D. Prowse, J. D. Reist, J. E. Hobbie, L. M. J. Levesque, and W. F.
761 Vincent (2006), Climate change effects on aquatic biota, ecosystem structure and
762 function, *AMBIO*, *35*(7), 359–369, doi:10.1579/0044-
763 7447(2006)35[359:CCEOAB]2.0.CO;2.

764 Yang, M., F. E. Nelson, N. I. Shiklomanov, D. Guo, and G. Wan (2010), Permafrost
765 degradation and its environmental effects on the Tibetan Plateau: A review of
766 recent research, *Earth-Science Reviews*, *103*(1–2), 31–44,
767 doi:10.1016/j.earscirev.2010.07.002.

768 Yoshikawa, K., and L. Hinzman (2003), Shrinking thermokarst ponds and groundwater
769 dynamics in discontinuous permafrost near Council, Alaska, *PERMAFROST AND*
770 *PERIGLACIAL PROCESSES*, *14*(2), 151–160, doi:10.1002/ppp.451.

771 Yukimoto, S. et al. (2012), A New Global Climate Model of the Meteorological Research
772 Institute: MRI-CGCM3-Model Description and Basic Performance, *JOURNAL*
773 *OF THE METEOROLOGICAL SOCIETY OF JAPAN*, *90A*(SI), 23–64,
774 doi:10.2151/jmsj.2012-A02.

775 Zhang, T. (2005), Influence of the seasonal snow cover on the ground thermal regime:
776 An overview, *REVIEWS OF GEOPHYSICS*, *43*(4), doi:10.1029/2004RG000157.

777 Zhang, T., J. Heginbottom, R. Barry, and J. Brown (2000), Further statistics on the
778 distribution of permafrost and ground ice in the Northern Hemisphere, *Polar*
779 *Geography*, *24*, 126–131.

780 Zhang, Y., W. Chen, and D. W. Riseborough (2008), Transient projections of permafrost
781 distribution in Canada during the 21st century under scenarios of climate change,
782 *GLOBAL AND PLANETARY CHANGE*, *60*(3-4), 443–456,
783 doi:10.1016/j.gloplacha.2007.05.003.

Zobler, L. (1986), *A World Soil File for Global Climate Modelling*, NASA Technical Memorandum 87802, NASA Goddard Institute for Space Studies, New York, New York, U.S.A.

9 Figure Captions

Figure 1: Data from the International Permafrost Association (IPA) map showing present day estimates of different permafrost zones. Only the continuous and discontinuous zones are used for comparison to models.

Figure 2: Soil column configurations used in various land models within the CMIP5 models. When legible, black dots indicate node depths. Bracketed number at base of columns indicates total number of layers.

Figure 3: CMIP5 model and Reanalysis climates for the IPCC reference period 1986-2005 represented as departures from the mean of the four reanalysis products.

Figure 4: (Upper panel) The range, maximum to minimum, of permafrost area under RCP8.5 via Surface Frost Index (SFI) and diagnosed directly from soil temperatures (TSL) for the period 1900-2099. The grey bar is indicative of the present-day area estimate. (Lower Panel) Permafrost area as computed by SFI plotted against TSL area, for each year of 1900-2099 for all RCP's. Both SFI and TSL data has a 10-year smoothing. Time progresses along each model line; the upper-right start of each line is the year 1900, the dot on the lines is 2000 and the lower-left end of each line is 2099.

Figure 5: Sensitivity of permafrost area to change in mean surface air temperature over the present-day permafrost region for all three diagnostic methods (TSL, SFI and KUD). Dots indicate model results and lines are linear fits. Across all cases the minimum r^2 value for RCP2.6 was 0.8 and 0.94 for RCP8.5. Colors indicate different models, as in Figure 4. Bold dashed line shows mean across all models

Figure 6: Mean change in surface air temperature over present day permafrost area. The number of models contributing to each RCP estimate is given in brackets. Shaded area is one standard deviation across models.

Figure 7: Projected change in sustainable permafrost area based on climate change from present day via the Surface Frost Index. Shaded areas represent 1 standard deviation across the CMIP5 models and the dashed black line is the model equivalent present day total area of continuous and discontinuous permafrost.

828
829 Figure 8: The number of climate trajectories with sustainable permafrost in 2099 based on
830 projected change in climate from present day reanalyses for each RCP scenario
831 according to the Surface Frost Index (SFI) method. The total number of models
832 available for each RCP is given in brackets in each panel. Present day observed
833 continuous and discontinuous permafrost is shown with grey shading.

834
835

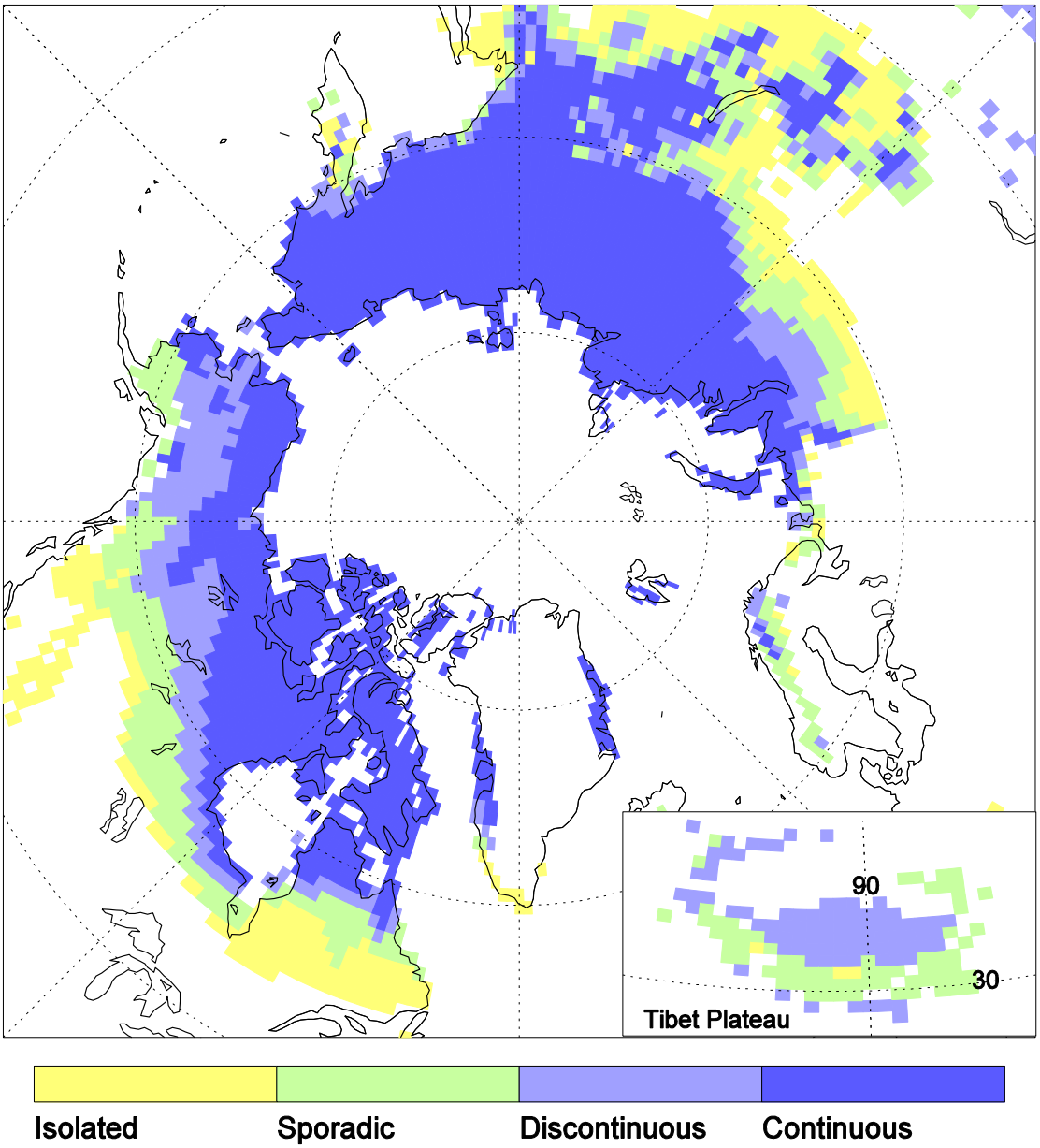

Figure 9: Data from the International Permafrost Association (IPA) map showing present day estimates of different permafrost zones. Only the continuous and discontinuous zones are used for comparison to models.

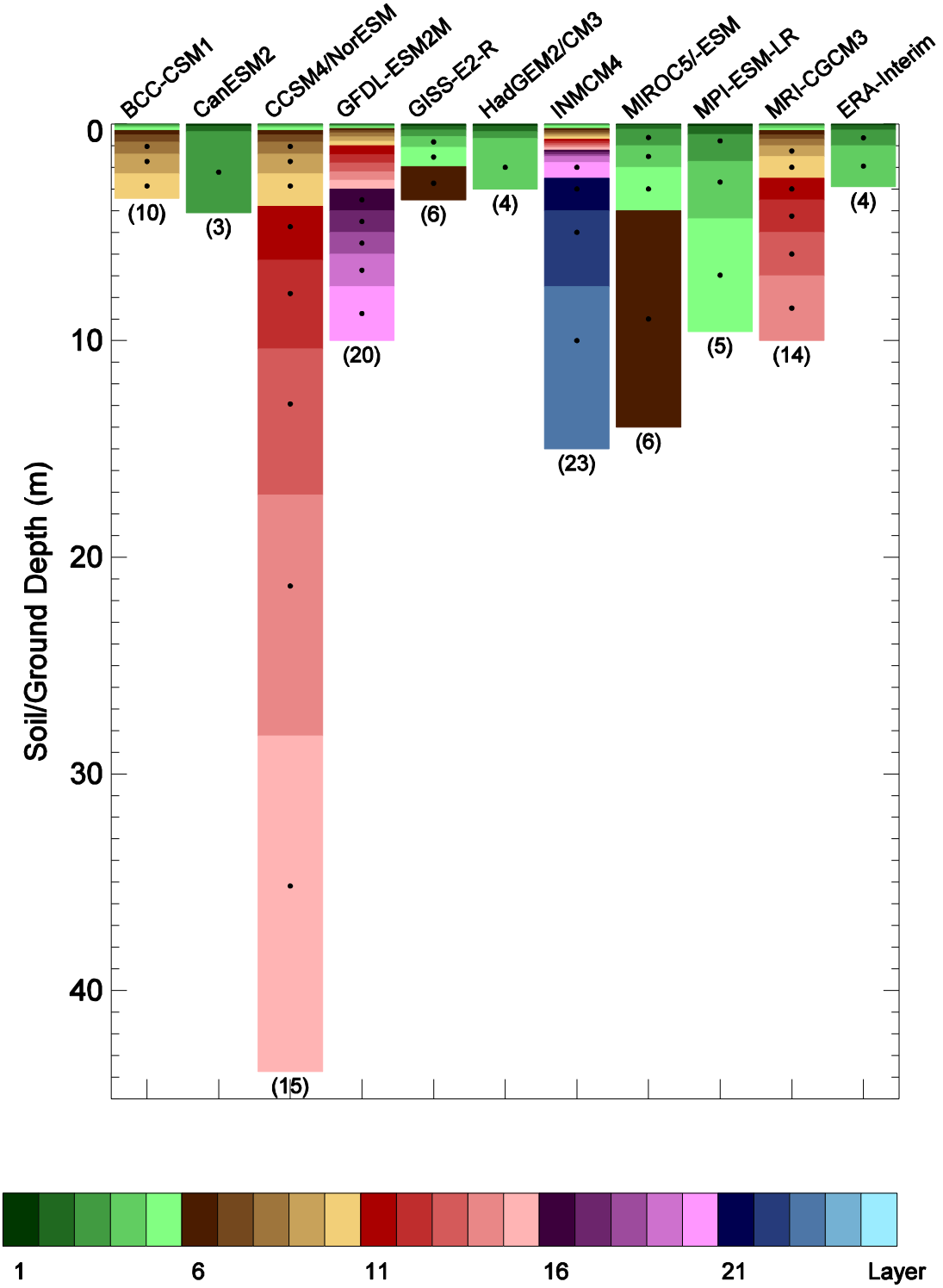

Figure 10: Soil column configurations used in various land models within the CMIP5 models. When legible, black dots indicate node depths. Bracketed number at base of columns indicates total number of layers.

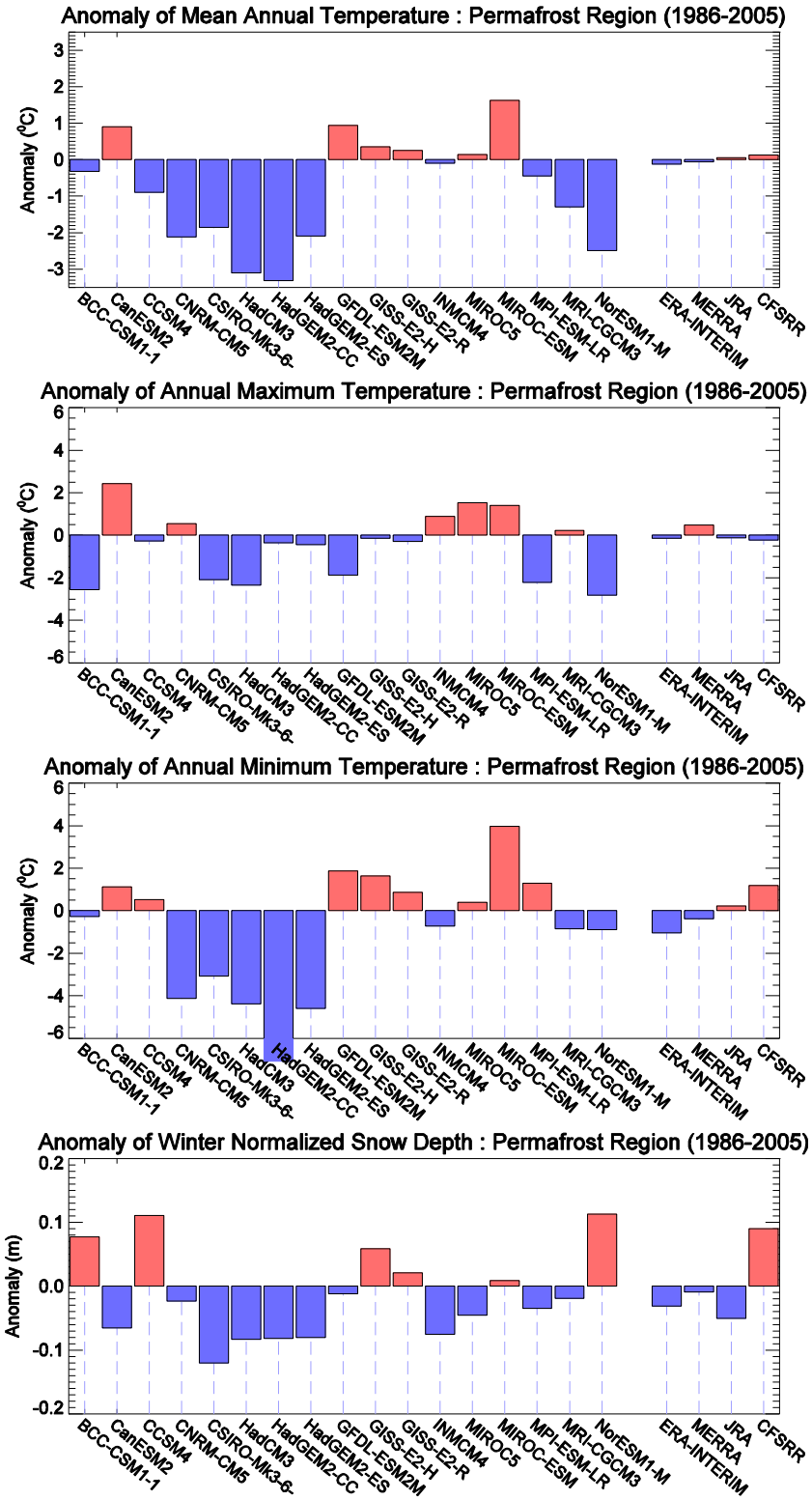

Figure 11: CMIP5 model and Reanalysis climates for the IPCC reference period 1986-2005 represented as departures from the mean of the four reanalysis products.

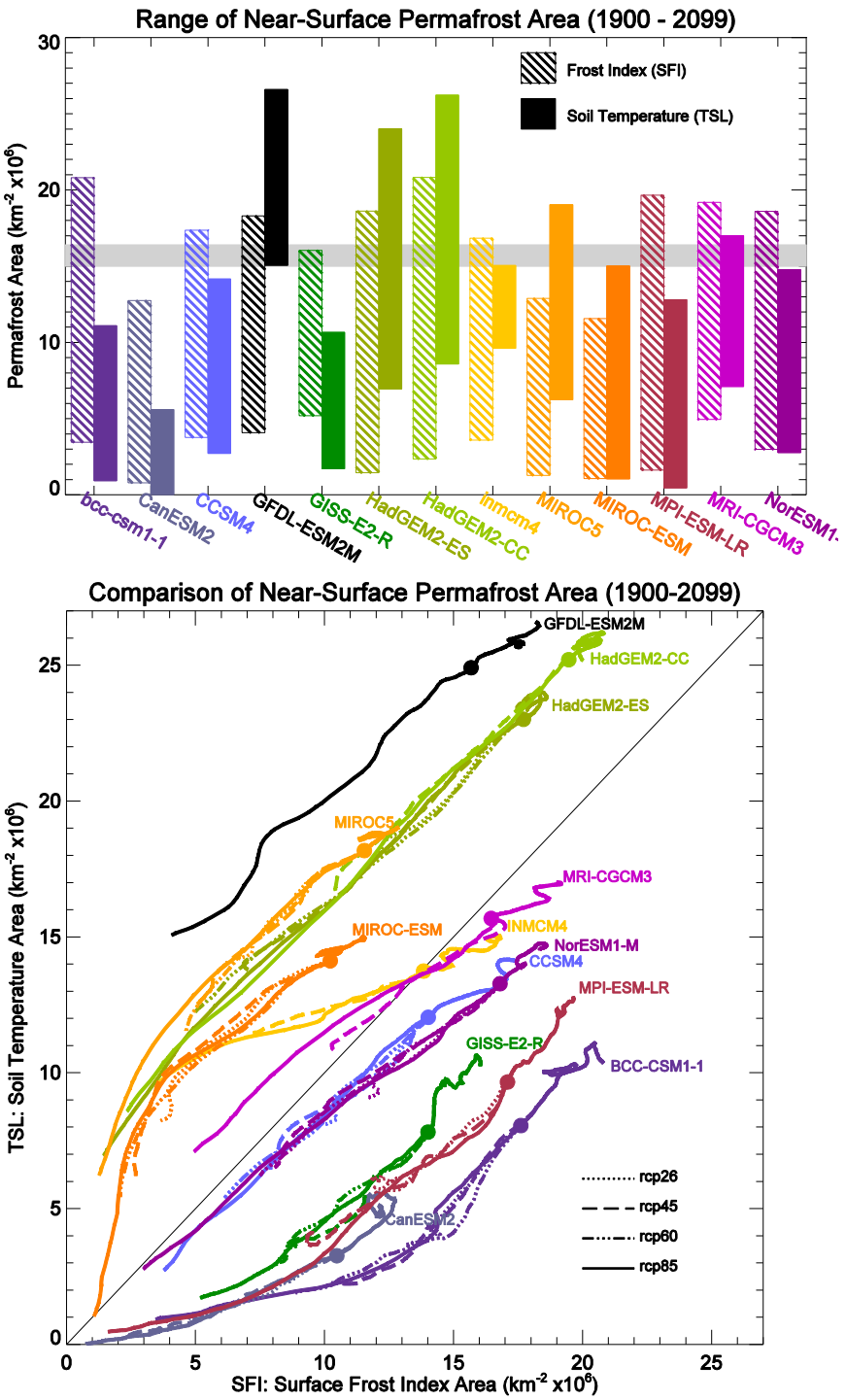

Figure 12: (Upper panel) The range, maximum to minimum, of permafrost area under RCP8.5 via Surface Frost Index (SFI) and diagnosed directly from soil temperatures (TSL) for the period 1900-2099. The grey bar is indicative of the present-day area estimate. (Lower Panel) Permafrost area as computed by SFI plotted against TSL area, for each year of 1900-2099 for all RCP's. Both SFI and TSL data has a 10-year smoothing. Time progresses along each model line; the upper-right start of each line is the year 1900, the dot on the lines is 2000 and the lower-left end of each line is 2099.

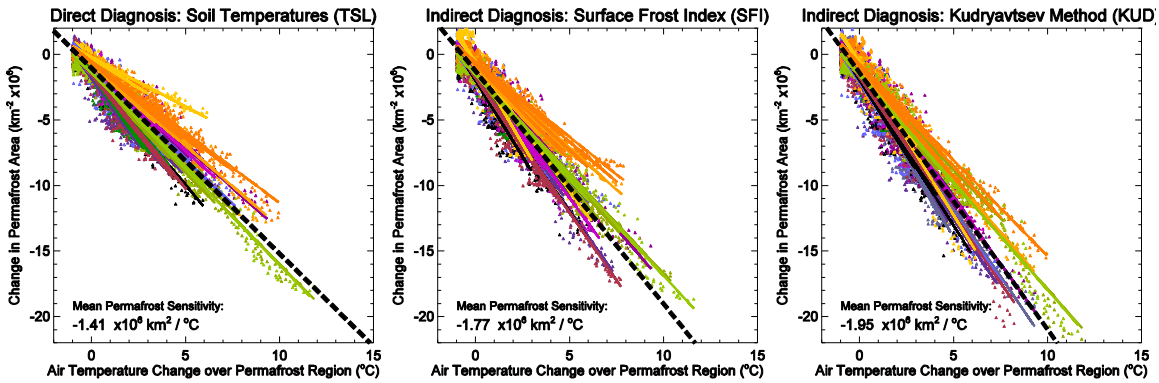

Figure 13: Sensitivity of permafrost area to change in mean surface air temperature over the present-day permafrost region for all three diagnostic methods (TSL, SFI and KUD). Dots indicate model results and lines are linear fits. Across all cases the minimum r^2 value for RCP2.6 was 0.8 and 0.94 for RCP8.5. Colors indicate different models, as in Figure 4. Bold dashed line shows mean across all models

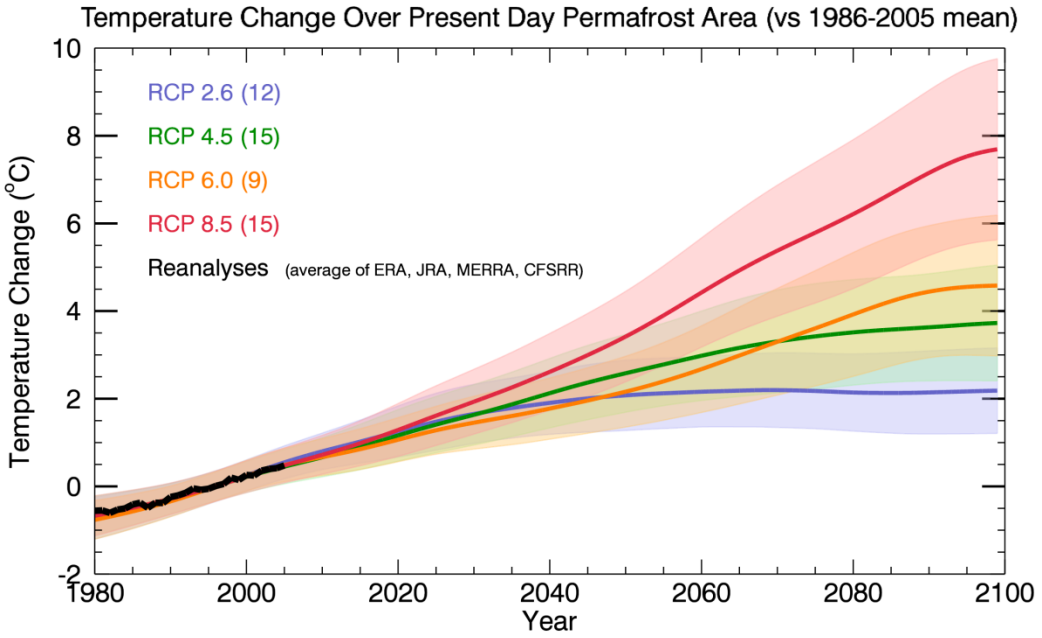

Figure 14: Mean change in surface air temperature over present day permafrost area. The number of models contributing to each RCP estimate is given in brackets. Shaded area is one standard deviation across models.

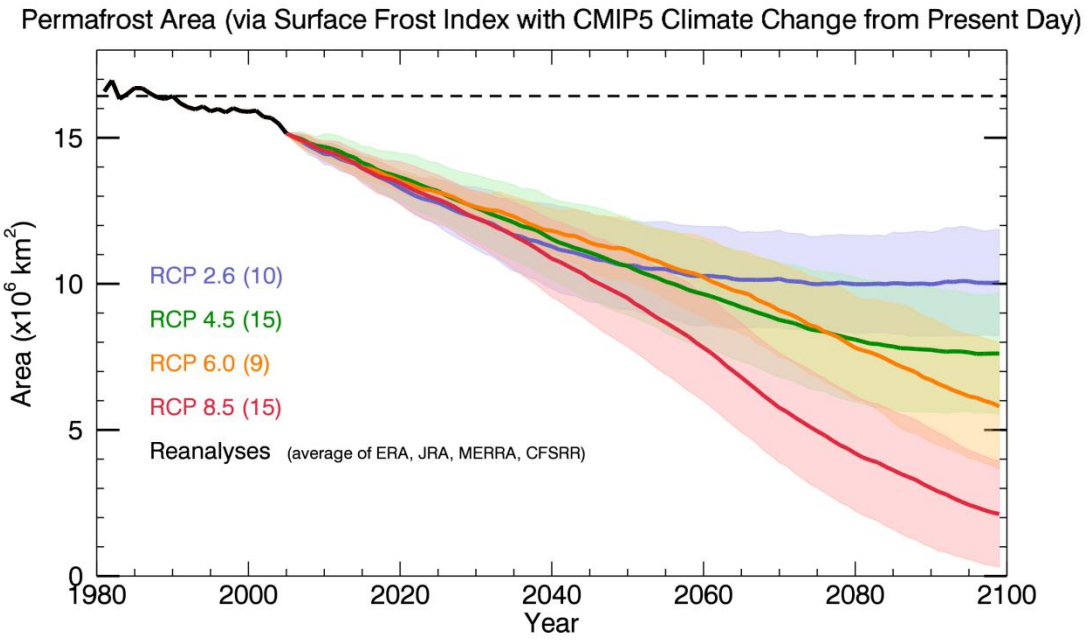

Figure 15: Projected change in sustainable permafrost area based on climate change from present day via the Surface Frost Index. Shaded areas represent 1 standard deviation across the CMIP5 models and the dashed black line is the model equivalent present day total area of continuous and discontinuous permafrost.

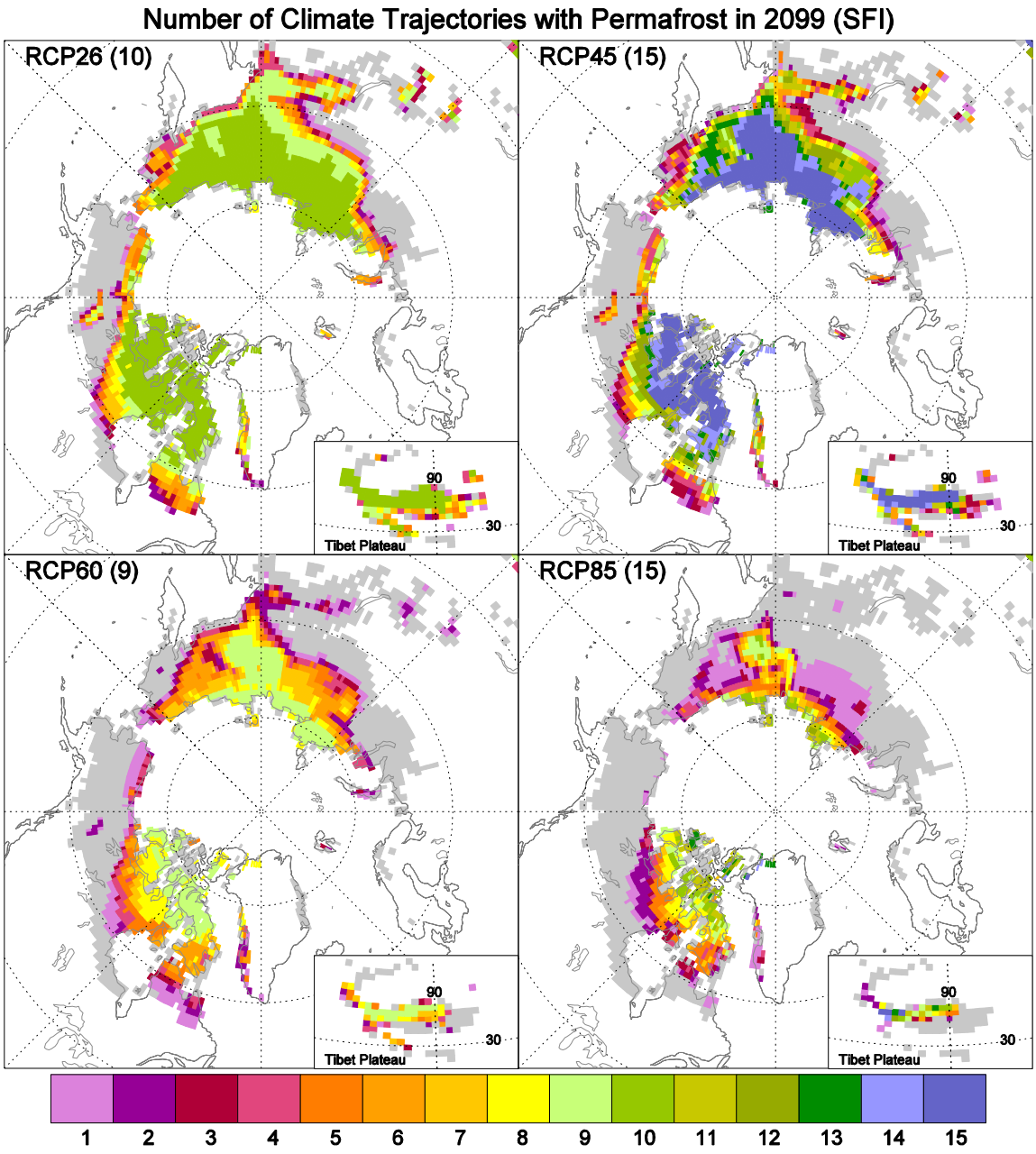

Figure 16: The number of climate trajectories with sustainable permafrost in 2099 based on projected change in climate from present day reanalyses for each RCP scenario according to the Surface Frost Index (SFI) method. The total number of models available for each RCP is given in brackets in each panel. Present day observed continuous and discontinuous permafrost is shown with grey shading.

10 Tables

Table 1: Model Characteristics

Model Name	Air Temp. (°C) *	MST:Soil Temp. (°C) *	Snow Depth Factor (m) *	Resolution (°Lat × °Lon)	Land Model	Snow Scheme Structure **	No. Soil Layers	Depth of Soil (m)	Model References
BCC-CSM1	-8.63	-0.18	0.408	2.8 × 2.8	BCC_AVIM1	Multi-Layer	10	3.43	[*Ji*, 1995; *BCC*, 2012]
CanESM2	-7.40	-6.71	0.266	2.8 × 2.8	CLASS2.7	Bulk Layer	3	4.10	[*Verseghy*, 2000]
CCSM4	-9.20	-1.49	0.442	0.9 × 1.25	CLM4	Multi-Layer	15	43.74	[*Oleson et al.*, 2010; *Lawrence et al.*, 2011]
CNRM-CM5	-10.43	-	0.308	1.4 × 1.4	SURFEX	Bulk-Layer	F/R	-	[*Boone et al.*, 2000; *LeMoigne et al.*, 2009]
CSIRO-Mk3.6-1	-10.17	-	0.211	1.875 × 1.875	CSIRO	Multi-Layer	5	4.60	[*Gordon et al.*, 2002]
GFDL-ESM2M	-7.37	-7.57	0.319	2.0 × 2.5	LM3	Multi-Layer	23	10.00	*Dunne et al.*, 2012
GISS-E2-H	-7.96	-	0.390	2.0 × 2.5	Model II-LS	Composite	6	3.50	[*Rosenzweig and Abramopoulos*, 1997]
GISS-E2-R	-8.05	-5.04	0.352	2.0 × 2.5	Model II-LS	Composite	6	3.50	[*Rosenzweig and Abramopoulos*, 1997]
HadCM3	-11.41	-	0.248	2.24 × 3.75	MOSES2.2	Implicit	4	3.00	[*Essery et al.*, 2001]
HadGEM2-CC	-11.62	-8.83	0.249	1.24 × 1.875	MOSES2.2	Implicit	4	3.00	[*Essery et al.*, 2001]
HadGEM2-ES	-10.40	-7.53	0.251	1.24 × 1.875	MOSES2.2	Implicit	4	3.00	[*Essery et al.*, 2001]
INMC M4	-8.40	-4.55	0.256	1.5 × 2.0	-	Bulk-Layer	20	15.00	[*Volodin and Lykosov*, 1998a, 1998b]
MIROC5	-8.17	-6.74	0.286	1.4 × 1.4	MATSIRO	Multi-Layer	6	14.00	[*Takata et al.*, 2003]
MIROC-ESM	-6.68	-4.12	0.340	2.8 × 2.8	MATSIRO	Multi-Layer	6	14.00	[*Takata et al.*, 2003]
MPI-ESM-LR	-8.75	-7.67	0.296	1.875 × 1.875	ECHAM5	Composite-SG	5	9.58	[*Roeckner et al.*, 2003]
MRI-CGCM3	-9.60	-3.16	0.312	1.125 × 1.125	HAL	Multi-Layer	14	10.00	[*Yukimoto et al.*, 2012]
NorESM1-M	-10.80	-3.24	0.444	1.875 × 2.5	CLM4	Multi-Layer	15	43.74	[*Oleson et al.*, 2010; *Lawrence et al.*, 2011]
Reanalyses									
CFSRR	-8.18	-	0.421	0.312 × 0.312	Noah	Composite	4	4.00	[*Ek et al.*, 2003; *Saha et al.*, 2010]
ERA-Interim	-8.43	-	0.300	0.7 × 0.7	TESSEL	Bulk-Layer	4	2.89	[*Viterbo et al.*, 1999]
JRA	-8.26	-	0.281	1.125 × 1.125	SiB	Composite	F/R	-	[*Sellers et al.*, 1986; *Sato et al.*, 1989]
MERRA	-8.37	-	0.322	0.50 × 0.66	Catchment	Multi-Layer	6	10.00	[*Koster et al.*, 2000]

* : Mean over present day continuous and discontinuous permafrost area for years 1986-2005 if data was available
** : According to scheme of Slater et al., [2001]
F/R : A Force-Restore scheme is used in which there are only 2 “layers” i.e. daily and seasonal thermal stores
Composite-SG : a shifting vertical grid of snow into soil is used in the thermal calculation depending on snow depth

Table 2: The sensitivity of permafrost area to changes in air temperature over the region of present day observed permafrost, under RCP8.5 forcing. Units are 10^6 km^2/°C

Model	TSL	SFI	KUD
BCC-CSM1	-1.58	-2.02	-2.13
CanESM2	-1.18	-1.72	-2.01
CCSM4	-1.34	-1.54	-2.02
CNRM-CM5	-	-	-
CSIRO-Mk3.6-1	-	-	-
GFDL-ESM2M	-1.69	-2.05	-2.23
GISS-E2-H	-	-	-
GISS-E2-R	-1.75	-1.88	-1.87
HadCM3	-	-	-
HadGEM2-CC	-1.47	-1.54	-1.64
HadGEM2-ES	-1.46	-1.52	-1.63
INMC M4	-0.75	-1.97	-2.32
MIROC5	-1.24	-1.27	-1.67
MIROC-ESM	-1.08	-1.14	-1.46
MPI-ESM-LR	-1.75	-2.07	-2.09
MRI-CGCM3	-1.32	-1.97	-1.97
NorESM1-M	-1.27	-1.66	-1.99

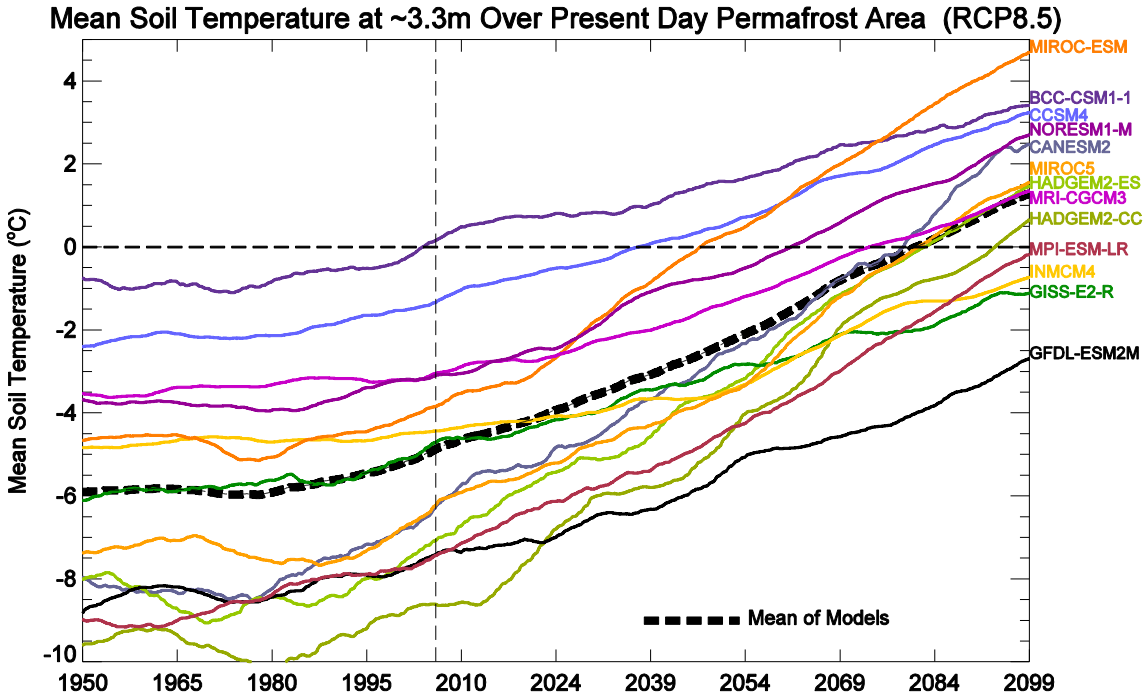

Additional Figure: Mean annual soil temperature at approximately 3.3m for all points within the present day observed continuous and discontinuous permafrost region (see Figure 1)